Research Square

Preprints are preliminary reports that have not undergone peer review.
They should not be considered conclusive, used to inform clinical practice,
or referenced by the media as validated information.

A new design method of winding tension considering thick-wall effect for composite overwrapped pressure vessel

Y. Jiang

2731752093@qq.com

Chaohu University

K. Jiang

Chaohu University

X. Y. Xu

Chaohu University

Research Article

Keywords: Thick-wall effect, Composite overwrapped pressure vessel, Winding tension, Residual stress, Hydrogen Storage

Posted Date: October 23rd, 2026

DOI: https://doi.org/10.21203/rs.3.rs-11121307/v1

License: This work is licensed under a Creative Commons Attribution 4.0 International License.
Read Full License

Additional Declarations: No competing interests reported.

A new design method of winding tension considering thick-wall effect for composite overwrapped pressure vessel

Y. Jiang[1*], K. Jiang[1,2], X.Y. Xu[1]

[1]School of Mechanical Engineering, Chaohu University, Hefei, Anhui, China, 238024

[2]Institute of Process Equipment and Control Engineering, Zhejiang University of Technology, Hangzhou, China, 310023

Abstract

Due to the thick-wall effect, the stress decreases from the inner-most to the outer-most layer in high pressure composite overwrapped pressure vessel (COPV) and results in low utilization ratio of fiber strength for outer layers. In this work, an analytical solution for the residual stress from winding tension is derived. Based on this analytical solution, a design method for winding tension is proposed to mitigate the thick-wall effect. In this method, the winding tension is designed to make the residual stress gradually increase from inside to outside layers. Thus the total stress, including the residual stress from winding tension and the service stress from the inner pressure, is uniformly distributed in the thickness direction and eliminates the thick-wall effect. The result of this method is validated and compared with other method. It is seen that the new method can produce uniform stress distribution and improve the mechanical performance of COPV.

Keywords: Thick-wall effect; Composite overwrapped pressure vessel; Winding tension; Residual stress; Hydrogen Storage.

* Corresponding author. E-mail address: 2731752093@qq.com

1. Introduction

Fossil fuel plays an important role in the total volume of energy consumption across the World. However, fossil fuel always produces carbon dioxide and other pollutants, which are considered to be the causes of warm house effect and environmental problems. Hydrogen is seen as an alternative for fossil fuel thanks to its recyclability, zero pollution and high energy density. Hydrogen has become a top priority of energy development strategy in most countries. Hydrogen fuel cell vehicle (HFCV) is a promising application scenario [1]. However, it is easy for hydrogen to leak, explode or even cause catastrophic event, so how to safely store hydrogen has become important for the development of efficient, safe and low-cost HFCVs [2]. For its excellent performance, composite overwrapped pressure vessel (COPV) is the most popular carrier for hydrogen.

To increase the travelling distance of HFCV, the nominal working pressure of COPV increases from 20 MPa to 70 MPa or even more. As the nominal working pressure increases, the thickness of composite increases to bear more stress. According to the radius-to-thickness ratio, shells can be classified into thin-wall and thick-wall shells. When the ratio is larger than 10, it is thin wall. When the ratio is smaller than 10, it is thick wall. The mechanical behaviors of thick wall will be different from those of thin wall. The most obvious difference is that in thick wall the stress and strain will show gradient through thickness. The stress in the composite decreases from the inner-most to outer-most layer. It is observed in Roh [3] that the stress in the inner-most layer bears 30% higher stress than the outer-most layer. According to the failure criterion of composite material, the stress state in the inner-most layer satisfies the fiber failure criterion first, while the stress state in the outside layers has not reached the threshold of failure, which means that the capacity of the fiber in the outside layers is not utilized to full extent, thereby reducing the mechanical performance of composite. To reduce the

thick-wall effect, the hoop layers mainly for hoop stress will be placed closer to the liner to bear more stress by some manufacturers. By this setting, space between layers is easily created in the transitional part from the dome to the cylinder. The space acts as defect and decreases the mechanical performance of COPV. Thus for high pressure COPV, the thick-wall effect through the wall is very important and must be taken into consideration in design.

To have better understanding of the stress distribution through the wall, the analytical solution for the stress distribution in COPV is necessary. The elastic solution for anisotropic cylinder is given by Lekhnitskii [4]. Based on Lekhnitskii's solution, Roy [5] has presented a simple and efficient design method for thick-wall composite cylinders. In their work, micromechanics and macromechanics are integrated by simple relations to enable the designers to instantly study the sensitivity of the micromechanical variables on the final design. Zu [6] presented a three-dimensional elasticity analysis on multi-layered thick-wall COPV. An exact solution to stresses of the metal liner and each anisotropic layer is given based on Lekhnitskii's solution and the generalized plane strain assumption. To reduce the weight of COPV, Zu [7] proposed a simplified method for designing isotensoid pressure vessels with unequal polar opening, using non-geodesic trajectories. An approximate three-dimensional elasticity solution is given for an infinite, thick, orthotropic as well as laminated circular cylindrical shell subjected to distributed pinch load [8]. An approach based on the exact solution of the three-dimensional problems of the theory of elasticity for certain cases is proposed [9]. The problem of thick-wall filament wound pipe subjected to outer pressure is solved analytically [10]. The failure prediction of different lay-ups and loading conditions is given by the analytical solution. The mechanical behaviors of thick-wall filament wound composite tube are studied by strength of material, analytical solution, finite element method and experimental

measurement [11]. Based on the theory of the three-dimensional thick-wall cylinder combined with Hashin failure criterion and damage evolution theory of composite materials, an analytical model for the progressive failure analysis of fiber reinforced thermoplastic pipes under internal pressure is proposed [12]. In this model the nonlinear stress-strain relationship of materials and the change in the winding angle caused by deformation are considered. Jia [13-14] set up a three-dimensional finite element model for thick-wall COPV, in which progressive damage constitutive model is adopted to predict damage evolution, failure mode and burst pressure. Islam [15] set up a finite element model to predict the burst pressure of high pressure COPV. In the model, the WCM Plugin is utilized to deal with the winding angle and thickness variation of composite layer on the domes. The accuracy of the finite element model is validated by analytical solution. Noor [16] studied the effects of variation in the lamination and geometric parameters of multi-layered composite cylinders on the accuracy of the static responses.

Previous studies [17] suggested that the quality of the filament wound composite cylinder is affected by the processing conditions. The residual stress induced by winding tension and curing is an important factor affecting the mechanical behavior of COPV. The residual stress can be optimized by winding tension and curing process to improve the performance of COPV. The winding tension can affect the volume of fiber, the stress distribution in composite and the liner, the burst pressure and fatigue life of COPV [18-20]. The influences of winding tension on the physical and mechanical properties of glass-fiber reinforced polymeric composite tube was studied by Mertiny [21]. Based on the elastic theory of cylindrical shells and the theory of composite laminates, a prediction model for the residual stress of the simplified round composite barrel for rail-gun is proposed by Yin [22]. Geng [23] studied the residual stresses induced in fiber pre-stressed

composite by both theoretical and numerical methods. Good agreement has been obtained between theoretical and numerical results. The results showed that the level of induced residual stresses within the composite depends not only on fiber pretension level, but also on the composite elastic properties. Kang [24] proposed a reverse derivation method to design the winding tension based on the residual stress model of the composite cylinder. The simple model of residual stress is established based on the superposition principle. The design method of winding tension is to guarantee that the hoop wound cylinder with an inner liner has a uniform residual stress. The results indicates that the model can be used to estimate the residual stresses and design the winding tension. An analytical model [25] is proposed to predict the through-thickness residual stresses and warpage of a composite part during the curing process without extensive resin characterization. Kang [26] proposed an algorithm to design the winding tension, in which the deformation of mandrel, radial and circumferential stresses of winding layers under external pressure are obtained through analysis on the basis of anisotropic composite elastic theory and isotropic thick-wall cylinder elastic theory. Based on the temperature differential method and the element deletion method [27], a model of hollow composite flywheel, which could successfully simulate the process of pretension when the composite material is wound, is built. After iterative computations, a better pretension design of the carbon fiber is provided [28]. A three-dimensional thermo-chemo-mechanical model [29] for the curing of the composite shell was established based on a resin test. The changes of temperature, curing degree, residual stress, and strain during the solidification of the composite shell were investigated. Han [30] studied the thermal curing residual stresses and its resultant distortions on filament-wound egg-shaped pressure-resistant shells under different structural parameters.

From the above-mentioned works, it is seen that most of the works are related to three-dimensional theoretical solution and pretension of COPV. In this work, the thick-wall effect in COPV is studied first. Then an analytical solution for residual stress generated from winding tension is derived. Based on this analytical solution, a new design method for the winding tension is proposed. In this new method, the winding tension is designed to produce residual stress which can mitigate the stress gradient from the inner-most to outer-most layers caused by thick-wall effect. Thus a nearly uniform total stress distribution through thickness is formed in the composite. Consequently, the outside and inside layers bear the same level of stress and reach the failure criterion simultaneously, exploiting the strength of all layers to the full extent and improving the mechanical performance of COPV.

The first part of this work is devoted to an introduction. The thick-wall effect in COPV is studied in Section 2. The derivation of the analytical solution of the residual stress from winding tension is introduced in Section 3. The new design method for the winding tension is detailed in Section 4. Section 5 is to validate the new method by numerical method. Section 6 is the conclusion.

2. Thick-wall effect in COPV

Thick-wall effect becomes more obvious in COPV as the thickness of composite increases. In order to design the winding tension to mitigate the thick-wall effect, the stress distribution along the thickness direction should be studied first. To get precise stress distribution along the thickness direction, a three-dimensional finite element model is set up.

2.1 Three-dimensional finite element model

In this work, a type III COPV with nominal working pressure 70MPa is studied. Thanks to the axisymmetric structure of COPV, a 5 degree of the COPV in the

circumferential direction is modeled with cyclic symmetric boundary conditions to save time cost of computation, as shown in Fig. 1. In the model, to get more accurate stress distribution along thickness direction, several layers of continuum shell elements SC8R are used to represent composite, instead of a single layer of conventional shell elements S4R . 528 C3D8R elements are used for the liner and 2728 SC8R elements for the composite. There are totally 6788 nodes in the model. 20 MPa pressure is applied on the inner surface of the COPV. The composite is carbon fiber T700 strengthened epoxy. The anisotropic material parameters for composite are listed in Tab. 1. The layup sequence of the composite is $[90_2/\pm 16]_{21}/90_2$. The elasto-plastic material parameters of aluminum alloy 6061T6 for the liner are shown in Tab. 2. The total thickness of the outside composite is 26.66 mm. Each two layers ($\pm\theta$) of composite are represented with one layer of element in thickness. The thickness of the liner is 8 mm. On the two domes of the COPV, there are only helical layers. The fiber angle θ and the thickness of each layer t_f change as the radius r for different location on the dome varies, and can be predicted by Eqs. (1) and (2), according to the netting theory. The local material coordinate system and the thickness of layer is defined for each location.

$$\theta = \arcsin(r_0 / r) \tag{1}$$

$$t_f = \frac{R\cos[\arcsin(r_0 / R)]}{r\cos[\arcsin(r_0 / r)]} t_{f\theta} \tag{2}$$

In these equations, r_o and R are the outer radii of the pole hole and the cylinder part of COPV respectively. $t_{f\theta} = 0.31\,\text{mm}$ is the thickness of the two layers ($\pm\theta$) as a whole. The material orientation is defined in the local coordinate system for each element.

2.2 Results and discussion

By the above three-dimensional finite element model, the stress analysis is performed. The fiber stress distribution in the hoop layers is plotted versus the axial distance for different layers, in Fig. 2. The vertical axis is the stress σ_{11} in fiber direction.

The horizontal axis is the layer number counting from the inner-most to the outer-most layer. It is shown that the stress nearly remains constant for each layer. It is also seen that the stress decreases from the inner-most layer to the outer-most layer, which can be explained by the thick-wall effect. Also the difference between two neighboring layers gradually decreases from outside to inside layers. In order to more obviously show the thick-wall effect, the fiber stress in the middle plane of COPV versus the layer number is plotted in Fig. 3. From the result, the highest value of the fiber stress 203 MPa comes from the inner-most layer, while the lowest value from the outer-most layer is 136 MPa, which is only 67% of the highest value and in good agreement with Ref. [11].

The stress σ_{22} is plotted in Fig. 4. The values at the middle plane for each layer are plotted in Fig. 5. From the figures, It is seen that σ_{22} is very small compared with the fiber stress σ_{11}. This is caused by the fact that the stiffness in the fiber direction is two orders higher than in the vertical direction, shown in Tab. 1. Most of the stress in axial direction of COPV is taken by the helical layers. The highest value of σ_{22} is 8.68 MPa, while the lowest value is 7.2 MPa or 83% of the highest value. It could be said that the thick-wall effect is also observed in σ_{22}.

From the above analysis, the thick-wall effect is obvious for σ_{11} and σ_{22} in hoop layers. σ_{11} in the outer-most hoop layer can be only 67% of the inner-most hoop layer. It means that when the fiber failure criterion is satisfied in the inner-most hoop layer, 33% of the strength in the outer-most hoop layer is not utilized, which of course will affect the burst pressure of COPV. This explains the reason why the increase in the number of layers does not result in linear increase of burst pressure of the COPV, when the thickness reaches a certain level.

3. Analytical solution for residual stress

To design the winding tension of composite layer, it is very important to clarify the relationship between the residual stress and winding tension. In this work, an analytical solution for residual stress generated from the winding tension of composite layer is derived for Type III COPV. Before the derivation, assumptions are made as follows:

(1) No friction exists between composite layers, or composite and the mandrel.

(2) The composite layers are in full and continuous contact. No slide between composite layers during winding.

(3) The effects of the gravity, temperature difference and axial stresses during winding are neglected.

(4) No plastic deformation. During the winding process, the mandrel and the composite layer experience linear elastic deformation. Thus the whole model can be considered to be a linear system, which makes superposition method applicable.

(5) The whole model is assumed to be axisymmetric.

Based on the above assumptions, a simple thick wall cylinder model with a metal liner is shown in Fig. 6. In the cylindrical mandrel with the filament winding structure, the outer surface of the mandrel and the inner surface of the winding layer comes into close contact because of the external pressure caused by the winding tension. The radial displacement and stress maintain continuous surface contact. Hence, we establish an equation to calculate the stress in the composite layer and the mandrel. The body of the mandrel should meet the balanced equation:

$$\frac{d\sigma_{1r}}{dr}+\frac{\sigma_{1r}-\sigma_{1\theta}}{r}=0 \tag{3}$$

Here σ_{1r} and $\sigma_{1\theta}$ are the radial and hoop stress in the mandrel.

According to the thick wall cylinder theory, the radial displacement and stress in the mandrel are as follows:

$$\begin{cases} u_{1r} = Ar + \dfrac{B}{r} \\ \sigma_{1r} = E_1\left(\dfrac{1}{1-v_1}A - \dfrac{1}{1+v_1}\dfrac{B}{r^2}\right) \end{cases} \tag{4}$$

Here u_{1r} and σ_{1r} are the radial displacement and stress in the mandrel. E_1 is the elasticity modulus, ν_1 is the Poisson's ratio of the mandrel. A and B are real constants, which can be determined by the boundary condition $\sigma_{1r} = 0$ on inner surface $r=a$ and $\sigma_{1r} = -p_1$ on outer surface $r=b$ of the mandrel. p_1 is the pressure on the mandrel outer surface generated from the winding layer. Thus we have

$$\begin{cases} A = \dfrac{1-v_1}{E_1}\dfrac{p_1}{\left(\dfrac{a^2}{b^2}-1\right)} \\ B = \dfrac{1+v_1}{E_1}\dfrac{p_1}{\left(\dfrac{1}{b^2}-\dfrac{1}{a^2}\right)} \end{cases} \tag{5}$$

The radial stiffness of the mandrel K is defined as:

$$K = \frac{\sigma_{1r}}{u_{1r}}\Big|_{r=b} = \frac{(b^2-a^2)E_1}{b\left(b^2(1-v_1)+a^2(1+v_1)\right)} \tag{6}$$

For the winding layer, the stress and strain relation was expressed as

$$\begin{cases} \varepsilon_{2r} = \dfrac{1}{E_{2r}}\sigma_{2r} - \dfrac{v_{2\theta}}{E_{2\theta}}\sigma_{2\theta} \\ \varepsilon_{2\theta} = \dfrac{1}{E_{2\theta}}\sigma_{2\theta} - \dfrac{v_{2r}}{E_{2r}}\sigma_{2r} \end{cases} \tag{7}$$

Here $\sigma_{2r}, \sigma_{2\theta}$ are the radial and circumferential stresses in the winding layer, $\varepsilon_{2r}, \varepsilon_{2\theta}$ being the radial and circumferential strains. $v_{2r}, v_{2\theta}$ are the Poisson's ratios, $E_{2r}, E_{2\theta}$ being the Young's modulus in r and θ direction. These parameters can be obtained by Eq. (8).

$$\begin{cases} E_{2r} = 1/\overline{C}_{11}, \quad E_{2\theta} = 1/\overline{C}_{22} \\ v_{2\theta} = -\overline{C}_{12}/\overline{C}_{22}, \quad v_{2r} = -\overline{C}_{12}/\overline{C}_{11} \end{cases} \tag{8}$$

Here $\overline{C}_{11}, \overline{C}_{22}, \overline{C}_{12}$ are the compliance matrix components for $\pm\theta$ winding layers and can be obtained by Eq. (9).

$$\begin{Bmatrix} \overline{C}_{11} \\ \overline{C}_{22} \\ \overline{C}_{12} \\ \overline{C}_{66} \end{Bmatrix} = \begin{bmatrix} m^4 & n^4 & 2m^2n^2 & 4m^2n^2 \\ n^4 & m^4 & 2m^2n^2 & 4m^2n^2 \\ m^4n^2 & m^2n^2 & m^4+n^4 & -4m^2n^2 \\ 2mn^3 & -2m^3n & 2(m^3n-mn^3) & m^3n-mn^2 \end{bmatrix} \begin{Bmatrix} C_{11} \\ C_{22} \\ C_{12} \\ C_{66} \end{Bmatrix} \tag{9}$$

Here $m = \cos\theta, n = \sin\theta$.

$$C_{11} = \frac{1}{E_L}, C_{22} = \frac{1}{E_T}, C_{12} = -\frac{v_T}{E_T} = -\frac{v_L}{E_L}, C_{66} = \frac{1}{G_{LT}} \tag{10}$$

are compliance matrix components. E_L, E_T are Young's modulus in longitudinal direction and transverse direction respectively. G_{LT} is shear modulus. v_L, v_T are Poisson's ratios in longitudinal and transverse plane respectively.

Because of actual deformation, using small deformation theory, the winding layer displacement and strain satisfied the following relations:

$$\begin{cases} \varepsilon_{2r} = \dfrac{\mathrm{d}u_{2r}}{\mathrm{d}r} \\ \varepsilon_{2\theta} = \dfrac{u_{2r}}{r} \end{cases} \tag{11}$$

Here u_{2r} is the radial displacement in the winding layer. Using the above Eqs. (7) and (11), we obtained the stress expression in the winding layer:

$$\begin{cases} \sigma_{2r} = \left[u'_{2r} + \dfrac{v_{2\theta}}{1-v_{2\theta}v_{2r}} \times \left(\dfrac{u_{2r}}{r} + v_{2r}u'_{2r} \right) \right] E_{2r} \\ \sigma_{2\theta} = \dfrac{E_{2\theta}}{1-v_{2\theta}v_{2r}} \left(\dfrac{u_{2r}}{r} + v_{2r}u'_{2r} \right) \end{cases} \tag{12}$$

The balance equation should be satisfied, i.e.

$$\frac{\mathrm{d}\sigma_{2r}}{\mathrm{d}r}+\frac{\sigma_{2r}-\sigma_{2\theta}}{r}=0 \tag{13}$$

Substituting Eq. (12) into Eq. (13) yields:

$$u_{2r}^{''}+\frac{u_{2r}^{'}}{r}-\frac{\beta^2}{r^2}u_{2r}=0 \tag{14}$$

where $\beta=\sqrt{\frac{E_{2\theta}}{E_{2r}}}$. The common solution to Eq. (14) is

$$u_{2r}=c_1r^{\beta}+c_2r^{-\beta} \tag{15}$$

where c_1 and c_2 are real constants to be determined

$$\begin{aligned}\sigma_{2r}&=c_1S_1r^{\beta-1}-c_2S_2r^{-\beta-1}\\ \sigma_{2\theta}&=c_1S_3r^{\beta-1}+c_2S_4r^{-\beta-1}\end{aligned} \tag{16}$$

Here $S_1=\frac{\beta+v_{2\theta}}{1-v_{2r}v_{2\theta}}E_{2r}, S_2=\frac{\beta-v_{2\theta}}{1-v_{2r}v_{2\theta}}E_{2r}, S_3=\frac{1+\beta v_{2r}}{1-v_{2r}v_{2\theta}}E_{2\theta}, S_4=\frac{1-\beta v_{2r}}{1-v_{2r}v_{2\theta}}E_{2\theta}$

The boundary conditions on the inner and outer surface of winding layer are:

$$\begin{aligned}\sigma_{2r}\,|_{r=b}&=\sigma_{1r}\,|_{r=b}\\ \sigma_{2r}\,|_{r=r_j}&=-p_2\end{aligned} \tag{17}$$

Here p_2 is the radial pressure generated from winding tension outside. Substituting Eq. (16) into Eq. (17) yields:

$$\begin{cases}c_1=-\dfrac{H_2(\frac{r_j}{b})^{2\beta}}{H_1S_2+H_2S_1\left(\frac{r_j}{b}\right)^{2\beta}}\dfrac{1}{r_j^{\beta-1}}p_2\\ c_2=-\dfrac{H_1(r_j)^{\beta+1}}{H_1S_2+H_2S_1\left(\frac{r_j}{b}\right)^{2\beta}}p_2\end{cases} \tag{18}$$

Here $H_1=Kb-S_1, H_2=Kb+S_2$ and K is defined in Eq. (6). Substituting Eq. (18) into Eq. (16) yields:

$$\begin{cases} \sigma_{2r} = -\dfrac{H_1S_2 + H_2S_1\left(\dfrac{r}{b}\right)^{2\beta}}{H_1S_2 + H_2S_1\left(\dfrac{r_j}{b}\right)^{2\beta}}\left(\dfrac{r}{r_j}\right)^{-\beta-1} p_2 \\ \sigma_{2\theta} = \dfrac{H_1S_4 - H_2S_3\left(\dfrac{r}{b}\right)^{2\beta}}{H_1S_2 + H_2S_1\left(\dfrac{r_j}{b}\right)^{2\beta}}\left(\dfrac{r}{r_j}\right)^{-\beta-1} p_2 \end{cases} \tag{19}$$

The remaining hoop stress is concerned with the external pressure and the radius of the winding layer. The radial stress produced by the winding tension increased with the progress of the winding process, and simultaneously the remaining hoop stress reduced.

$$p_2 = \int_{r_j}^{r_o} \frac{T_w(r)}{hBr}\mathrm{d}r \tag{20}$$

Here h is thickness of single layer, B is the width of winding tap. $T_w(r) = F_j\cos\theta$ is the hoop component of winding tension. F_j is the winding tension in the fiber direction. θ is the winding angle. Substituting Eq. (20) into Eq(19) yields:

$$\Delta\sigma_{2\theta} = \frac{H_1S_4 - H_2S_3\left(\dfrac{r}{b}\right)^{2\beta}}{H_1S_2 + H_2S_1\left(\dfrac{r_j}{b}\right)^{2\beta}}\left(\frac{r}{r_j}\right)^{-\beta-1}\int_{r_j}^{r_o}\frac{T_w(r)}{hBr}\mathrm{d}r \tag{21}$$

Based on the superposition principal, the residual stress can be calculated as the summation of the initial tension and the reduction of the tension.

$$\sigma_{2\theta} = \frac{T_w(r)}{hB} + \Delta\sigma_{2\theta} \tag{22}$$

Substituting Eq. (21) into Eq. (22) yields:

$$\sigma_{2\theta} = \frac{T_w(r)}{hB} + \frac{H_1S_4 - H_2S_3\left(\dfrac{r}{b}\right)^{2\beta}}{H_1S_2 + H_2S_1\left(\dfrac{r_j}{b}\right)^{2\beta}}\left(\frac{r}{r_j}\right)^{-\beta-1}\int_{r_j}^{r_o}\frac{T_w(r)}{hBr}\mathrm{d}r \tag{23}$$

To simplify the calculation in Eq. (23), the integration part can be replaced by summation as:

$$\sigma_{2\theta}=\frac{T_w(r)}{hB}+\frac{H_1S_4-H_2S_3\left(\frac{r}{b}\right)^{2\beta}}{H_1S_2+H_2S_1\left(\frac{r_j}{b}\right)^{2\beta}}\left(\frac{r}{r_j}\right)^{-\beta-1}\sum_{m=j+1}^{n}\frac{T_w(r_m)}{Br_m} \tag{24}$$

Eq. (24) can be written in matrix form as:

$$\begin{bmatrix}\sigma_{2\theta}^1\\ \sigma_{2\theta}^2\\ \cdots\\ \cdots\\ \sigma_{2\theta}^n\end{bmatrix}=\frac{1}{B}\begin{bmatrix}1/h & d_{12} & \cdots & \cdots & d_{1n}\\ 0 & 1/h & d_{23} & \cdots & d_{2n}\\ \cdots & 0 & 1/h & \cdots & \cdots\\ \cdots & \cdots & 0 & 1/h & \cdots\\ 0 & \cdots & \cdots & 0 & 1/h\end{bmatrix}\begin{bmatrix}T_w(r_1)\\ T_w(r_2)\\ \cdots\\ \cdots\\ T_w(r_n)\end{bmatrix} \tag{25}$$

Here $\sigma_{2\theta}^i$ is the residual hoop stress for ith layer generated from the winding tension of the layers from the ith layer to the nth layer. Here d_{ij} is the coefficient for winding tension of the jth layer to the ith layer and can be given in Eq. (26).

$$d_{ij}=\frac{H_1S_4-H_2S_3(\frac{r}{r_{j-1}})^{2\beta}}{H_1S_2+H_2S_1(\frac{r_j}{r_{j-1}})^{2\beta}}(\frac{r}{r_j})^{-\beta-1}\frac{1}{r_j} \tag{26}$$

Here r_{j-1} is the inner radius for jth layer. For j=1, $r_{j-1}=b$. Based on Eq. (25), the winding tension for each layer can be easily obtained as follows:

$$\begin{bmatrix}T_w(r_1)\\ T_w(r_2)\\ \cdots\\ \cdots\\ T_w(r_n)\end{bmatrix}=\mathrm{B}\begin{bmatrix}1 & d_{12} & \cdots & \cdots & d_{1n}\\ 0 & 1 & d_{23} & \cdots & d_{2n}\\ \cdots & 0 & 1 & \cdots & \cdots\\ \cdots & \cdots & 0 & 1 & \cdots\\ 0 & \cdots & \cdots & 0 & 1\end{bmatrix}^{-1}\begin{bmatrix}\sigma_{2\theta}^1\\ \sigma_{2\theta}^2\\ \cdots\\ \cdots\\ \sigma_{2\theta}^n\end{bmatrix} \tag{27}$$

By Eq. (27), if the residual stress for each layer is known, the winding tension for each layer can be easily obtained.

4. Design method of winding tension considering thick-wall effect

From section 2, we can see the thick-wall effect will affect the utilization ratio of the fiber strength especially for outside layers. In COPV, the hoop stress is mainly undertaken by the hoop layers with the axial stress by the helical layers. In the cylindrical part, the hoop stress is twice the axial stress. Thus, the number of hoop layers is approximately twice the number of helical layers, thereby covering two thirds of the total fiber volume. In this work, the design method of winding tension mainly focuses on the hoop layers with an expectation to reduce the fiber usage.

Usually, uniform residual stress method (URM) is used to design the winding tension. In URM, a uniform residual stress is pursued in the design. The later-wounded layer will pressurize the pre-wounded layer, thus reducing the residual stress in the pre-wounded layer. Therefore, to maintain a uniform residual stress field, the winding tension gradually decreases from the inner-most layer to the outer-most layer. With URM, according to the superposition principal, the summation of the residual stress from winding tension and service stress induced by inner pressure gradually decreases from the inner-most to the outer-most layer, resulting in a lower utilization ratio of fiber strength, shown in Fig. 7. In the figure, “Inner pressure” denotes the service stress caused by the pressure on the inner surface of the COPV. “Residual stress with URM” for the uniform residual stress caused by URM. “Total stress with URM” for the sum of the service stress and the uniform residual stress.

In this work, a design method considering thick-wall effect (denoted by TWE) is proposed. In TWE, the winding tension is designed to make the total stress caused by both winding tension and inner pressure uniform through the thickness direction, shown in Fig. 7. In figure 7, “Residual stress with TWE” stands for the residual stress generated from TWE. “Total stress with TWE” for the sum of the service stress and the residual

stress generated from TWE. Therefore, theoretically the fiber will reach the failure threshold simultaneously for all layers, hence greatly improving the mechanical performance of the COPV compared with the URM. In figure 7, the sum of the residual stress of each layer by TWE is kept equal to that by URM for fairness.

The main steps for TWE are listed as follows:

1. Set up the three-dimensional finite element model for the thick-wall COPV.
2. Calculate the fiber stress for each hoop layer under only inner pressure.
3. According to the fiber stress distribution through the thickness calculated in Step 2, based on superposition method the residual stress from winding tension is obtained so that a uniform total stress distribution exists in thickness direction.
4. Based on the residual stress from winding tension obtained in Step 3, the winding tension for each layer is calculated by Eq. (27).

5. Validation

To validate the method proposed in this work, TWE is applied to the design of the winding tension for high pressure COPV. The geometry of the COPV is the same as in Section 2. The fiber stress for each hoop layer is obtained from the three-dimensional finite element model, tabulated in Tab. 3. In the table, for hoop layers two layers of 90_2 are wounded together. The fiber stress in these two layers is the same. From the table, it is seen that from the first layer to the last layer the stress in fiber direction decreases from 203 MPa to 136 MPa. To adjust this non-uniform distribution, the residual stress from the winding tension for each hoop layer is designed as Tab. 4. To prevent the buckling of the fiber during winding, the stress should be tensile. A minimum 11 MPa is set for the residual stress of the first layer. For other layers, the residual stress is set to keep the sum of the stress under inner pressure and residual stress the same as the first layer. By this design, when the inner pressure and winding tension are added together, the total stress

for each layer is the same (214 MPa). Other values can also be assigned as the residual stress to reach the aim of uniform total stress in the fiber. The residual stress of each layer is not unique. After the residual stress is set for each layer, the winding tension for each layer should be calculated according to Eq. (27), tabulated in Tab. 5.

5.1 Simulation

To simulate the winding tension, the "element birth and death" method and thermal expansion [27] are utilized in this work. In the "element birth and death" method, all the composite layers are dead in the beginning of the simulation to mimic the status before winding. In the numerical method, the death of the element is realized by setting the stiffness of the material to be a value close to zero. When the winding process starts, the composite elements are activated layer by layer. In the commercial software, the elements are activated by changing the stiffness matrix from a nearly zero value to its normal value.

The winding tension of each layer is simulated by cooling effect, which will shrink the layer in the fiber direction. But the inside layers and the liner will prevent the shrinkage of the layer. Thus a winding tension is formed in the layer. Induced by different winding tension for different layers, the shrinkage of each layer will be different. The shrinkage of each layer is calculated by Eq. (28). Here ε_{11}^{i} is the strain in the fiber direction of the *i*th layer. The strain components in other two directions are set to be zero. The thermal coefficients in the fiber direction for each layer is set according to Eq. (29), in which ΔT_i is the temperature decrease for each layer. The coefficients in other two directions are set to be zero. To simplify the simulation, the temperature decrease ΔT_i of the whole model is set to be the same as -1℃. The thermal expansion coefficient for each layer is tabulated in Tab. 6. The uniform -1℃ temperature decease field is applied to the model layer by layer and solve the equation.

$$\varepsilon_{11}^{i} = \frac{T_w(r_i)}{hB}, \varepsilon_{22}^{i} = 0, \varepsilon_{33}^{i} = 0 \tag{28}$$

$$\alpha_{11}^{i} = \frac{\varepsilon_{11}^{i}}{\Delta T_i}, \alpha_{22}^{i} = 0, \alpha_{33}^{i} = 0 \tag{29}$$

5.2 Results and discussion

The total stress (the summation of the residual stress induced by winding tension and service stress from 20 Mpa inner pressure) in the fiber direction for each hoop layer with TWE is plotted and compared with URM in Fig. 9. In the figure, 'Total stress with TWE' denotes the total stress with the proposed method considering thick-wall effect, 'Total stress with URM' for the total stress with URM. From the figure, it can be seen that the total stress by the newly proposed method is more uniform than conventional uniform residual stress method. The thick-wall effect is obvious in the results by URM. In the new method, the stress is nearly uniform for each layer. The stress in the inner-most layer by URM is nearly 20% higher than that by TWE. That means the mechanical performance of COPV with winding tension designed with TWE will be better than that with URM. It is also observed that the total stress is not exactly uniform in each layer as designed with TWE. This is caused by the fact that the new method is based on superposition principal, for which liner system is required. While in the COPV, the liner is elastic-plastic material as shown in Tab. 2.

From this validation, we can say that by the new method proposed in this work, the thick-wall effect is not observed in the total stress. The new method is effective in the elimination of the thick-wall effect, thus improving the mechanical behaviors of composite in high pressure COPV.

6. Conclusion

Induced by thick-wall effect, the fiber direction stress decreases from inside layers to outside layers in high pressure composite overwrapped pressure vessel (COPV). The

strength of the fiber in the outside layers is not fully utilized. In this work, a new design method for winding tension is proposed to mitigate the thick-wall effect and improve the mechanical performance of COPV. The three-dimensional finite element model of COPV is set up to study the thick-wall effect first. The fiber stress distribution caused by inner pressure in thickness direction is obtained. An analytical solution for the residual stress generated from winding tension is derived. Based on the stress distribution, the residual stress by winding tension is designed to eliminate the thick-wall effect. Based on the relationship between the residual stress and the winding tension, the winding tension for each layer is designed. Finally a finite element model for the winding tension and inner pressure is set up to validate the newly proposed method. Some conclusions are drawn as follows:

1. As the thickness of COPV increases, the thick-wall effect becomes more obvious. Induced by the thick-wall effect, the strength of the fiber in the outer layers is not fully utilized. Thus it is very important to consider the thick-wall effect in the design of COPV.

2. An analytical solution for the residual stress from winding tension is derived. Based on the analytical solution, the winding tension can be easily designed from the known residual stress.

3. The new design method for winding tension is shown to be effective to mitigate the thick-wall effect and provide uniform total stress distribution in thickness direction compared with other method. Designed by this new method, the mechanical performance of COPV will be improved.

Funding Declaration

This work was supported by the Start-up funding for research of Chaohu University (KYQD-2024039).

REFERENCE

[1] Samid Khan, Ajay Kumar. Manufacturing challenges in advanced cylindrical composite pressure vessels for hydrogen storage: a comprehensive review. Energy Storage, 2025, 7(7):e70263.DOI:10.1002/est2.70263.

[2] Jiang Y, Wei ST, Xu P. Influences of filling process on the thermal-mechanical behavior of composite overwrapped pressure vessel for hydrogen. International Journal of Hydrogen Energy. 2020;45:23093-102.

[3] Roh HS, Hua TQ, Ahluwalia RK. Optimization of carbon fiber usage in Type 4 hydrogen storage tanks for fuel cell automobiles. International Journal of Hydrogen Energy 2013,38:12795-12802.

[4] SG L. Anisotropic plates. New York: Gorden and Breach, 1968.

[5] Roy AK, Tsai SW. Design of Thick Composite Cylinders. Journal of Pressure Veseel Technology. 1988;110:255-62.

[6] Zu L, Wang J, Li S. Analysis of multi-layered thick-walled filament-wound hydrogen storage vessels. International Journal of Hydrogen Energy. 2014;39:21083-96.

[7] Zu L, Koussios S, Beukers A. Design of filament-wound isotensoid pressure vessels with unequal polar openings. Composite structures. 2010;92:2307-13.

[8] Chandrashekhara K, Rao KSN. Approximate Elasticity Solution for A Long and Thick Laminated Circular Cylindrical Shell of Revolution. International Journal for Solids and Structures. 1997;34:1327-41.

[9] Grigorenko YM, Vasilenko AT, Pankratova ND. Computation of the stressed state of thickwalled inhomogeneous anisotropic shells. Soviet Applied Mechanics. 1974;10:523-8.

[10] Igor A. Guz, Marina Menshykova and Jeom Kee Paik. Thick-walled composite tubes for offshore applications: an example of stress and failure analysis for filament-wound multi-layered pipes. Ships and Offshore Structures 12.3-4(2015):304-322.

[11] Saeid Khadem Moshir, Suong V. Hoa, Farjad Shadmehri, Daniel Rosca, Ashraf Ahmed. Mechanical behavior of thick composite tubes under four-point bending. Composite Structures 242 (2020) 112097

[12] Yangyang Wang, Min Lou, Xin Zeng, Wenyi Dong, Sen Wang. Burst capacity of reinforced thermoplastic pipes based on progressive failure criterion. Ocean Engineering 234.4587(2021):109001.

[13] Lei Ge, Jikang Zhao, Hefeng Li, Jingxuan Dong, Hongbo Geng, Lei Zu, Song Lin, Xiaolong Jia, Xiaoping Yang. A three-dimensional progressive failure analysis of filament-wound composite pressure vessels with void defects. Thin-Walled Structures 199 (2024) 111858.

[14] Qian Zhang, Hui Xu, Xiaolong Jia, Lei Zu, Shuo Cheng, Huabi Wang. Design of a 70 Mpa type IV hydrogen storage vessel using accurate modeling techniques for dome thickness prediction. Composite Structures 236 (2020) 111915.

[15] M.M. Islam, M.F. Hossain, M.S. Rana, M.S. Ferdous. Burst pressure prediction of carbon/natural fiber and hybrid composite pressure vessels by theoretical and numerical analysis. Hybrid Advances 5 (2024) 100172.

[16] Noor AK, Burton WS, Peters JM. Assessment of computational models for multilayered composite cylinders. International Journal for Solids and Structures. 1991;27:1269-86.

[17] Cohen D, Mantell SC, Zhao L. The effect of fiber volume fraction on filament wound composite pressure vessel strength. Composites Part B: Engineering. 2001;32:413-29.

[18] Cohen D. Influence of filament winding parameters on composite vessel quality and strength. Composites Part A. 1997;28A:1035-47.

[19] Hashimoto H. Optimization of Wind-Up Tension of Webs Preventing Wrinkles and Slippage. Journal of Manufacturing Science and Engineering. 2009;131.

[20] Imamura T, Kuroiwa T, Takemoto TH. Development of hoop filament winding system with tension control. Transactions of the Japan Society of Mechanical Engineers Part C. 2003;69:906-13.

[21] Mertiny P, Ellyin F. Influence of the filament winding tension on physical and mechanical properties of reinforced composites. Composites Part A: applied science and manufacturing. 2002;33:1615-22.

[22] Dongmei Yin , Baoming Li, Hongcheng Xiao. Analysis for the residual prestress of composite barrel for railgun with tension winding. Defence Technology. 2020;16:893-9.

[23] Pei Geng, Qizhi Wang. Hoop winding tension design of thick-walled cylinder using superposition and unloading methods. Ships and Offshore Structures 2021; 16(2): 172-183.

[24] Chao Kang, Yaoyao Shi, Bo Deng, Tao Yu, Pengcheng Sun. Determination of residual stress and design of process parameters for composite cylinder in filament winding. Advances in Materials Science and Engineering. 2018:1-11.

[25] Zhenyi Yuan, Yongjun Wang, Xiongqi Peng, Junbiao Wang, Shengmin Wei. An analytical model on through-thickness stresses and warpage of composite laminates due to tool-part interaction. Composites Part B. 2016;91: 408-413.

[26] Kang Chao, Shi Yao-yao, He Xiao-dong, Yu Tao, Zhang Jun. Algorithm of winding tension for cylinder with thick-walled liner. Engineering Mechanics 2016;33(2):200-208.

[27] Yang X, Zupei S, Suyuan Y. Use elements "birth and death" method to analyze the multi-layer filament winding case. Journal of Mechanical Strength. 2005;27:526-9.

[28] Dong L, Sien M, Yanfeng L. Analysis based on temperature differential method and element deletion method of composite flywheel in tension winding. Energy Engineering. 2011;1:8-12.

[29] Linjiao Lu, Shengsheng Huan, Mengkai Lu, Tao Shen, Yanhui Tian, Jianying Hu, Jianke Du and Minghua Zhang. Three-dimensional thermo-chemo-mechnical coupled curing analysis for the filament wound composite shell. Polymers 2024, 16, 1643. https://doi.org/ 10.3390/polym16121643.

[30] Dawei Han, Chao Kang, Yuan Hu, Edmond Tobin, Ashish Vashishtha, Shuangni Tan, Zan Liu, Liping Wang, Zhiyang Gu, Jian Zhang. Evolution of curing residual stresses for filament-wound egg-shaped pressure-resistant shells considering viscoelastic properties. Polymer Composites. 2025; 46:285-306.

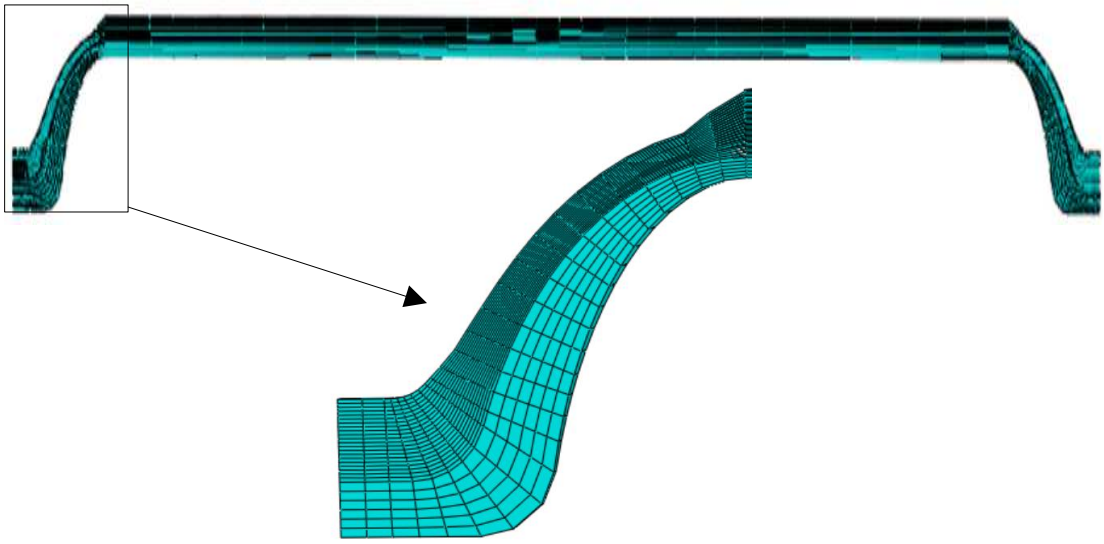


Fig. 1 The three-dimensional finite element model.

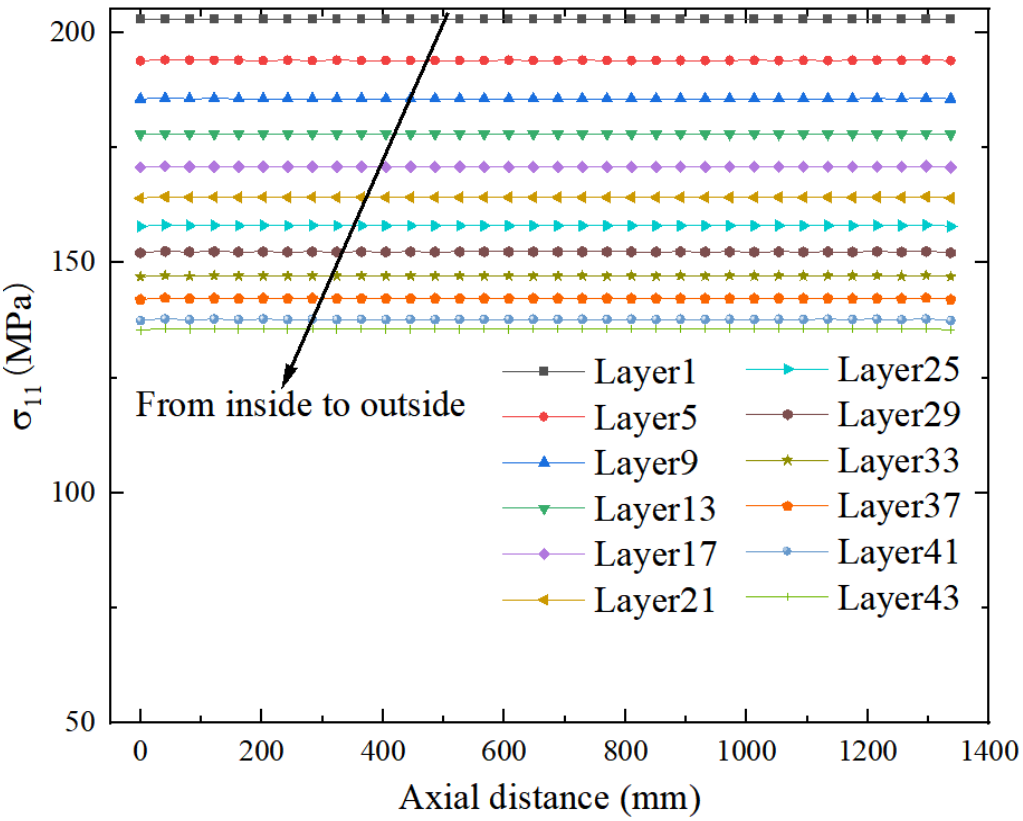


Fig. 2 The three-dimensional fiber stress distribution for the hoop layers.

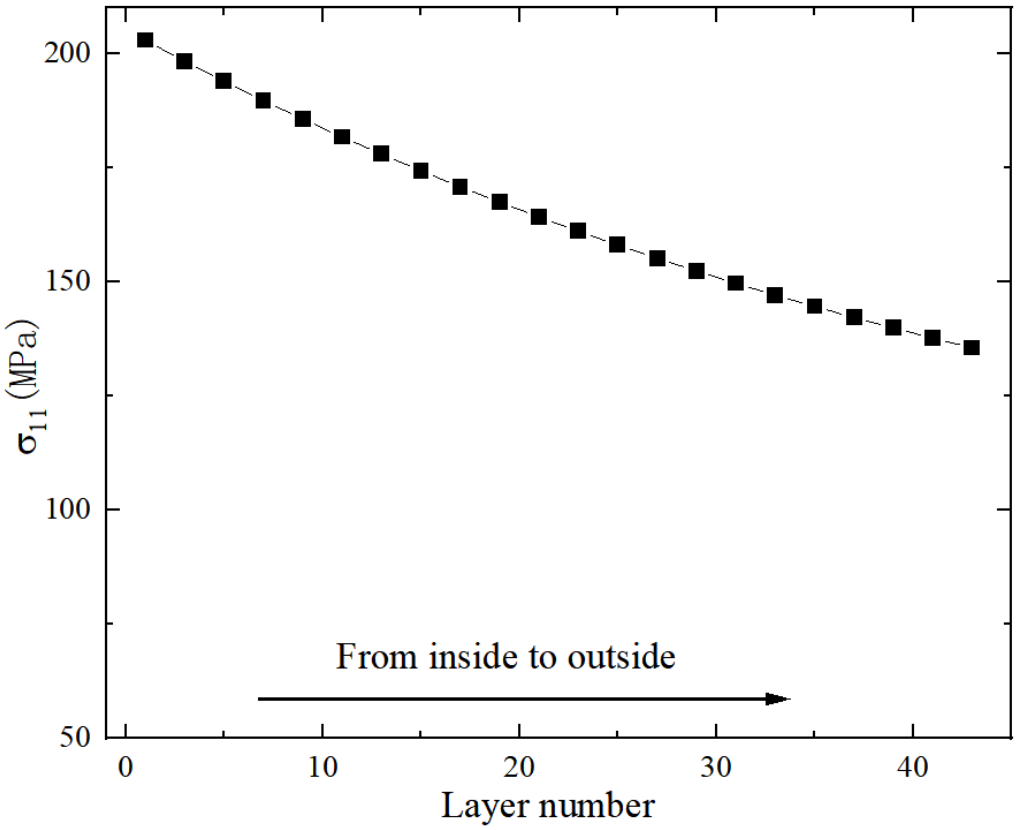


Fig. 3 The fiber stress variation through the thickness direction

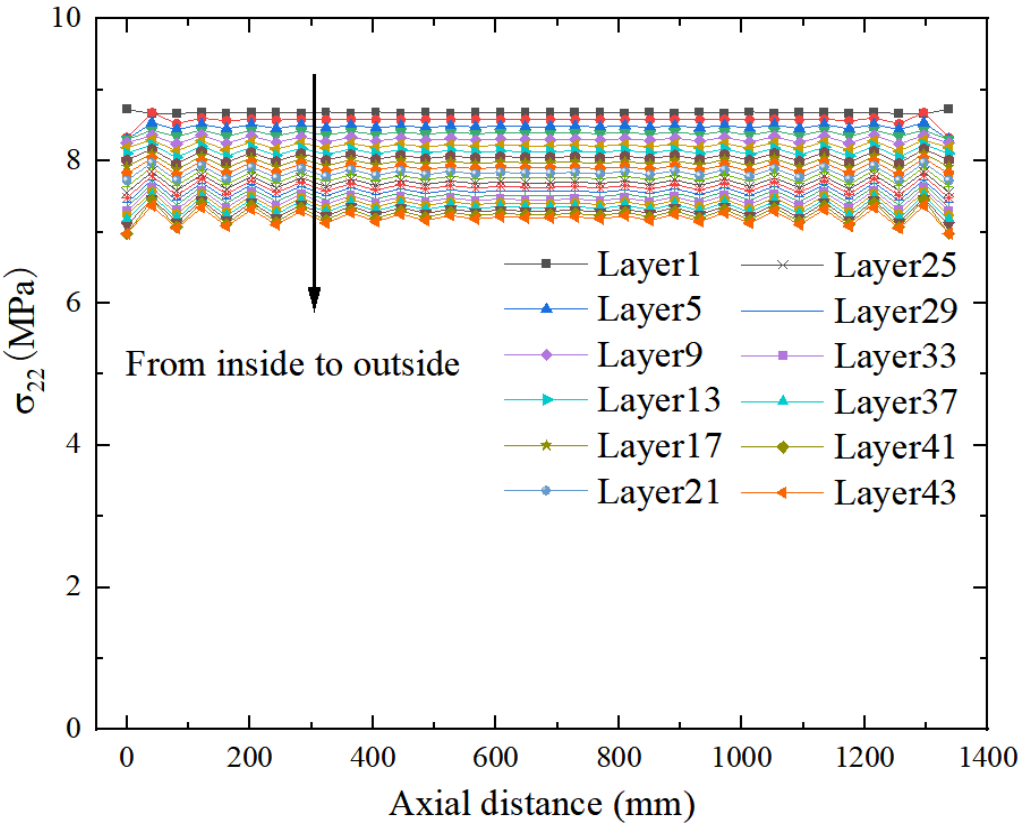


Fig. 4 The three-dimensional σ_{22} distribution for the hoop layers.

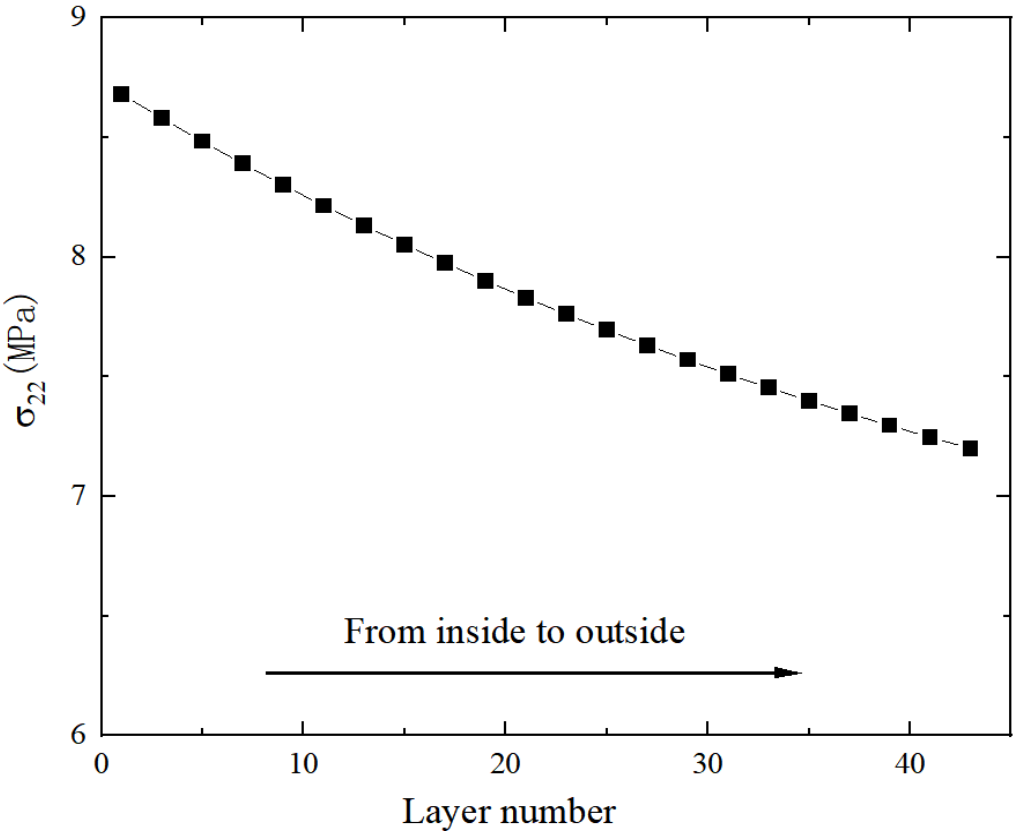


Fig. 5 The variation of σ_{22} through the thickness.

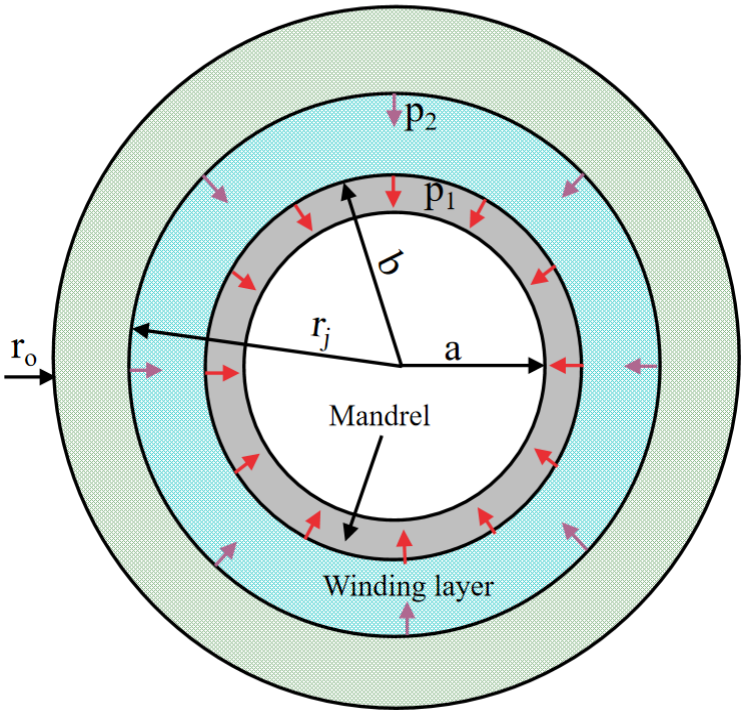


Fig. 6 The cross-section of wingding tension model.

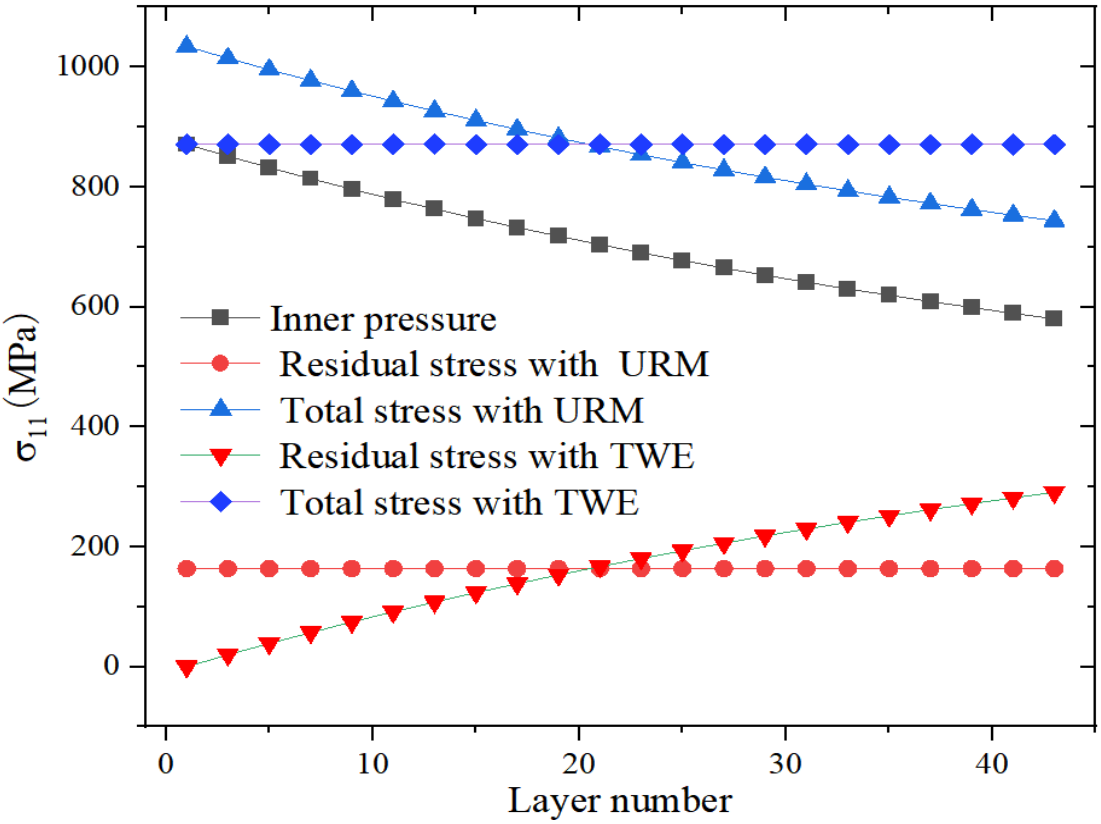


Fig. 7 Different winding tension design methods

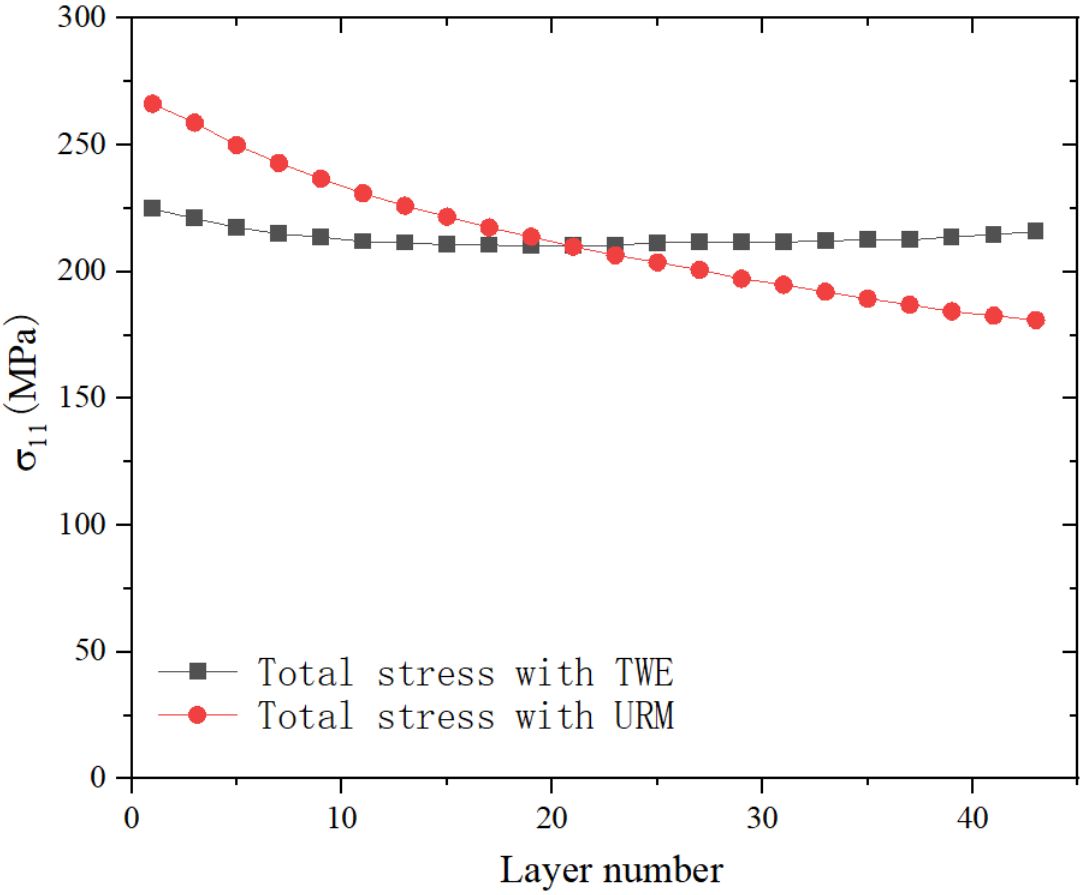


Fig. 8 The total stress at the middle plane versus the layer number by different methods

Tab. 1 Material property of composite

E_{11} (MPa)	E_{22}(MPa)	G_{12}(MPa)	G_{13}(MPa)	G_{23}(MPa)	v_{12}
134220	8180	4700	4700	2960	0.36

Tab. 2 Material property of aluminum alloy T6061

E(MPa)	v	σ_s(MPa)	σ_b(MPa)
70000	0.33	246	324

Tab. 3 The fiber stress for each hoop layer with only inner pressure

Layer No	1	3	5	7	9	11	13	15
σ_{11} (MPa)	203	198	194	190	186	182	178	174
Layer No	17	19	21	23	25	27	29	31
σ_{11} (MPa)	171	167	164	161	158	155	152	150
Layer No	33	35	37	39	41	43		
σ_{11} (MPa)	147	145	142	140	138	136		

Tab. 4 The residual stress for each hoop layer after winding

Layer No	1	3	5	7	9	11	13	15
σ_{11} (MPa)	11	16	20	24	28	32	36	40
Layer No	17	19	21	23	25	27	29	31
σ_{11} (MPa)	43	47	50	53	56	59	62	64
Layer No	33	35	37	39	41	43		
σ_{11} (MPa)	67	69	72	74	76	78		

Tab. 5 The primary winding tension for each hoop layer

Layer No	1	3	5	7	9	11	13	15
F_i (N)	258	263	264	267	270	274	278	283
Layer No	17	19	21	23	25	27	29	31
F_i (N)	284	290	292	295	297	300	304	303
Layer No	33	35	37	39	41	43		
F_i (N)	306	306	310	310	310	311		

Tab. 6 The thermal expansion coefficient in the fiber direction for each hoop layer

Layer No	1	3	5	7	9	11	13	15
$\alpha_{11}(\times 10^{-4}℃^{-1})$	4.13	4.21	4.24	4.28	4.33	4.39	4.47	4.55
Layer No	17	19	21	23	25	27	29	31

$\alpha_{11}(\times 10^{-4}℃^{-1})$	4.56	4.66	4.69	4.73	4.77	4.82	4.87	4.85
Layer No	33	35	37	39	41	43		
$\alpha_{11}(\times 10^{-4}℃^{-1})$	4.92	4.91	4.97	4.97	4.98	4.99		